Robotica: (2021) volume 39, pp. 699–717. © The Author(s), 2020. Published by Cambridge University Press.
doi:10.1017/S0263574720000673

Robust Multimode Flight Framework Based on Sliding Mode Control for a Rotary UAV

Abraham Villanueva†, Luis F. Luque-Vega‡, Luis E. González-Jiménez¶ and Carlos A. Arellano-Muro†

†*CINVESTAV-IPN Unidad Guadalajara, Zapopan, Jalisco, Mexico.*
E-mails: abrahamvn@gmail.com, carellano@gdl.cinvestav.mx
‡*Centro de Investigación, Innovación y Desarrollo Tecnológico CIIDETEC-UVM, Universidad del Valle de México, Tlaquepaque, Jalisco 45601, Mexico. E-mail: luis.luque@uvmnet.edu*
¶*Department of Electronics, Systems and Informatics, ITESO - The Jesuit University of Guadalajara, Tlaquepaque, Jalisco, Mexico.*

(Accepted June 19, 2020. First published online: July 24, 2020)

SUMMARY
This work presents a multimode flight framework control scheme for a quadrotor based on the super twisting algorithm. The controller design stages for six flight control modes are presented. The stability proof for each flight mode is carried out by means of Lyapunov functions, while the stability analysis for the complete control scheme, when a transition from one flight mode to another occurs, is demonstrated using the switching nonlinear systems theory. The performance of the proposed framework is shown in a 3D simulation environment considering a forest fire detection task, which takes into account external disturbances.

KEYWORDS: Sliding modes; Multimode flight control; Quadrotor; Switching dynamics.

1. Introduction

Unmanned aerial vehicles (UAVs), especially rotary UAVs, are becoming the mainstream in civilian realm for performing a wide range of applications involving monitoring, inspection, detection, recognition, and identification of different objects of interest. This is due to the advantages that this kind of aircrafts offers in comparison to others like vertical take-off and landing, hovering, and the ability to follow a sharp trajectory. One of the most popular multirotor today is the quadrotor. This multirotor is highly nonlinear, underactuated, and subject to disturbances and parameter uncertainties. Most of the research carried out on this platform have tackled the stabilization and the trajectory tracking problem. There are several interesting robust flight controllers proposed for solving the stabilization problem, for example, nested saturations controller,[1] super twisting control algorithm,[2] fuzzy control,[3] a backstepping approach taking into account the actuator faults,[4] among others. On the other hand, for the trajectory tracking problem, a feedback linearization controller with a high-order sliding mode differentiator[5] or observer,[6] a backstepping control with a sliding mode observer,[7] a combination of backstepping and sliding mode control,[8] a controller based on adaptive and sliding mode control,[9] and an adaptive backstepping controller based on invariant manifolds[10] have been applied with satisfactory results. Furthermore, some techniques from the intelligent control field such as neural networks with adaptive control,[11] or including sliding mode, control for robustness.[12] Also, fuzzy control for the trajectory tracking of quadrotors[13] under wind disturbances. In addition, the passivity approach through the inmmerse and invariance technique in combination with adaptive control

* Corresponding author. E-mail: luisgonzalez@iteso.mx

https://doi.org/10.1017/S0263574720000673 Published online by Cambridge University Press

was proposed by Zou and Meng.[14] As seen in the previous referenced works, and due to its robustness properties and ease of implementation, the sliding modes have been used in combination with other control algorithms, including an integral term to the control law,[15] or even for the control of formations of UAVs.[16]

All the aforementioned flight controllers are focused in one single flight mode; therefore, it represents a great challenge to design a multimode flight control system. Moreover, the commercial multirotor control boards include different flight modes to be selected by the user, depending on the task to develop by the rotorcraft.[17] In this regard, Bo et al.[18] present a modular designing method to describe the overall structure of simulation model of an UAV having different flight control modes using Stateflow, and combining with MATLAB graphical user interface, the remote control instruction. Also, Hongzhe et al.[19] proposed three flight control modes for an unmanned helicopter based on different design stages and gave the autonomous control algorithm and the smoothing method, while switching between remote control mode and stability augmentation mode. Boskovic and Mehra[20] proposed a framework for multimodal flight control based on the multiple mModels, switching and tuning methodology, and model-predictive control. In that work, it is shown that implementing robust mechanisms for switching between controllers for different flight modes is feasible and that the framework can be adapted for different switching strategies. There are a wide range of applications for multirotors such as forest fire detection, power line inspection, surveillance, and others which require the capability of having several and robust flight modes available.

Additionally, Villanueva et al.[21] presented a framework for a multimode flight control system for a quadrotor based on the super twisting control algorithm, which encompasses four flight modes. This work represents an extension of ref. [21] as the main framework of a multimode flight control system for a quadrotor based on the robust super twisting algorithm. This framework takes into account six different flight modes: manual position, altitude hold, GPS fixed, autonomous, manual velocity mode, and return to home. Furthermore, a state machine is defined to represent the transitions between the flight modes of the aircraft during the monitoring period, and the resulting controllable sequences of transitions are defined.

The paper is organized as follows: in the following section, the description of the quadrotor dynamics is presented. The design stages for the complete multimode flight framework are presented in Section 3. Then, Section 4 presents the stability analysis for each flight mode and for the complete system in the event of a transition from one flight mode to another. Simulation results illustrating the effectiveness of the proposed framework in the presence of external disturbances are given in Section 5 and some conclusions close the paper.

2. Quadrotor Dynamics

The dynamic model is derived under the following assumptions: the structure is supposed to be rigid and symmetrical, the center of mass and the body-fixed frame origin are assumed to coincide, and the propellers are supposed rigid. The equations describing the attitude and position of a quadrotor helicopter are basically those of a rotating rigid body with six degrees of freedom (DoF).[22] Let us consider two main reference frames: the earth-fixed frame E^E and body-fixed frame E^B which is fixed at the center of mass of the quadrotor.

The space orientation of the aircraft between E^B and E^E is given by the transformation velocity matrix $R(\Theta)$ and the rotation velocity matrix $M(\Theta)$[5] which are defined as

$$R(\Theta) = \begin{bmatrix} C_\psi C_\theta & C_\psi S_\theta S_\phi - S_\psi C_\phi & C_\psi S_\theta C_\phi + S_\psi S_\phi \\ S_\psi C_\theta & S_\psi S_\theta S_\phi + C_\psi C_\phi & S_\psi S_\theta C_\phi - C_\psi S_\phi \\ -S_\theta & C_\theta S_\phi & C_\theta C_\phi \end{bmatrix}$$

and

$$M(\Theta) = \begin{bmatrix} -S_\theta & 0 & 1 \\ C_\theta S_\phi & C_\phi & 0 \\ C_\theta C_\phi & -S_\phi & 0 \end{bmatrix}$$

where ψ, θ, and ϕ are the Euler angles of the vehicle with respect to the E^B frame, $C_i = cos(i)$, and $S_i = sin(i)$. The dynamic model is derived using Newton–Euler formalism in the body-fixed frame E^B, about the rotorcraft subjected to external forces ΣF_{ext} and moments ΣT_{ext} applied to the center

https://doi.org/10.1017/S0263574720000673 Published online by Cambridge University Press

of mass. Thus, the dynamic equations of motion are described by

$$\begin{aligned}\Sigma F_{ext} &= m\dot{V}_B + \Omega \times mV_B \\ \Sigma T_{ext} &= I\dot{\Omega} + \Omega \times I\Omega\end{aligned} \tag{1}$$

where m is the mass of the quadrotor, $I = diag(I_x, I_y, I_z)$ is the inertia matrix of the helicopter, V_B is the linear translational velocity, and Ω is the angular velocity. The external forces and moments are expressed in the body-fixed frame as

$$\begin{aligned}\Sigma F_{ext} &= F_{prop} - F_{aero} - F_{grav} \\ \Sigma T_{ext} &= T_{prop} - T_{aero} - T_{gyro}\end{aligned} \tag{2}$$

where $F_{prop} = col(0, 0, U_1)$ is the forces vector and $T_{prop} = col(U_2, U_3, U_4)$ is the moments vector produced by the propellers. $F_{grav} = mR(\Theta)^T G$ is the gravity effect force with $G = col(0, 0, 9.81)\ \mathrm{m/s^2}$, $F_{aero} = col(A_x, A_y, A_z)$, and $T_{aero} = col(A_p, A_q, A_r)$ are the aerodynamic forces and moments acting on the UAV, respectively. $T_{gyro} = \sum_{i=1}^{4} J(\Omega \times e_3)(-1)^{i+1}\omega_i$ defines the gyroscopic effects resulting from the propeller rotations. The inputs $U_i (i = 1, 2, 3, 4)$ are defined as

$$\begin{aligned}U_1 &= \sum\nolimits_{i=1}^{4} F_i \\ U_2 &= d(F_4 - F_2) \\ U_3 &= d(F_3 - F_1) \\ U_4 &= \frac{c}{b}\sum\nolimits_{i=1}^{4}(-1)^i F_i\end{aligned} \tag{3}$$

where d is the distance from the center of mass to the rotor shaft, c is the drag factor, J is the rotor inertia, and $F_i = b\omega_i^2$, $(i = 1, 2, 3, 4)$ is the force generated by the rotational speed of the motor ω_i and the thrust factor b. The aerodynamic functions A_j, $(j = x, y, z, p, q, r)$ are computed as $A_j = \frac{1}{2}\rho C_j W^2$ from the aerodynamic coefficients C_j, the air density ρ, and $W = \Omega - \Omega_{air}$, which is the velocity of the aircraft with respect to the air. Using (1) and (2), the equations describing the dynamics of the quadcopter can be expressed in the reference frame E_E as

$$\begin{aligned}&\ddot{X}_E = \tfrac{1}{m}R(\Theta)[F_{prop} - F_{aero}] - G, \\ &\ddot{\Theta} = [IM(\Theta)]^{-1}\begin{bmatrix} T_{prop} - T_{aero} - T_{gyro} - M(\Theta)\dot{\Theta}\times \\ IM(\Theta)\dot{\Theta} - I\left(\dfrac{\partial M(\Theta)}{\partial\theta}\dot{\theta} + \dfrac{\partial M(\Theta)}{\partial\phi}\dot{\phi}\right)\dot{\Theta}\end{bmatrix}\end{aligned} \tag{4}$$

and simplifying the matrix $M(\Theta)$ as the identity due to small variations of the attitude angles of the aircraft, we can express the following equations:

$$\begin{aligned}\ddot{x} &= \frac{U_1}{m}\left(S_\phi S_\psi + C_\phi S_\theta C_\psi\right) - A_x \\ \ddot{y} &= \frac{U_1}{m}\left(-S_\phi C_\psi + C_\phi S_\theta S_\psi\right) - A_y \\ \ddot{z} &= \frac{U_1}{m}\left(C_\phi C_\theta\right) - g - A_z \\ \ddot{\phi} &= \frac{1}{I_x}\left(U_2 + \left(I_y - I_z\right)\dot{\theta}\dot{\psi} + J\dot{\theta}\omega\right) - A_p\end{aligned} \tag{5}$$

https://doi.org/10.1017/S0263574720000673 Published online by Cambridge University Press

$$\ddot{\theta} = \frac{1}{I_y}\left(U_3 + (I_z - I_x)\,\dot{\phi}\dot{\psi} + J\dot{\phi}\omega\right) - A_q$$

$$\ddot{\psi} = \frac{1}{I_z}\left(U_4 + \left(I_x - I_y\right)\dot{\phi}\dot{\theta}\omega\right) - A_r,$$

where $S_{(\cdot)}$ and $C_{(\cdot)}$ are sine and cosine of the subindex, respectively.

Then, writing the system in the state-space form, and assigning $X = [x, \dot{x}, y, \dot{y}, z, \dot{z}, \phi, \dot{\phi}, \theta, \dot{\theta}, \psi, \dot{\psi}]^T$, we obtain the following state-space representation

$$\begin{aligned}
\dot{x}_1 &= x_2 \\
\dot{x}_2 &= \frac{U_1}{m}\left(S_{x_7}S_{x_{11}} + C_{x_7}S_{x_9}C_{x_{11}}\right) - A_2 \\
\dot{x}_3 &= x_4 \\
\dot{x}_4 &= \frac{U_1}{m}\left(-S_{x_7}C_{x_{11}} + C_{x_7}S_{x_9}S_{x_{11}}\right) - A_4 \\
\dot{x}_5 &= x_6 \\
\dot{x}_6 &= \frac{U_1}{m}\left(C_{x_7}C_{x_9}\right) - g - A_6 \\
\dot{x}_7 &= x_8 \\
\dot{x}_8 &= \frac{1}{I_x}\left(U_2 + \left(I_y - I_z\right)x_{10}x_{12} + Jx_{10}\omega\right) - A_8 \\
\dot{x}_9 &= x_{10} \\
\dot{x}_{10} &= \frac{1}{I_y}\left(U_3 + (I_z - I_x)\,x_8x_{12} + Jx_8\omega\right) - A_{10} \\
\dot{x}_{11} &= x_{12} \\
\dot{x}_{12} &= \frac{1}{I_z}\left(U_4 + \left(I_x - I_y\right)x_8x_{10}\right) - A_{12}
\end{aligned} \tag{6}$$

with $X = [x_1, x_2, ..., x_{12}]^T$.

3. Multimode Flight Control Design

The multimode flight control system considered for the rotary UAV provides six different flight modes: manual position, altitude hold, GPS fixed, autonomous, manual velocity mode, and return to home. Even though the six flight modes have a similar control structure, their main difference is the references that each flight mode requires and their corresponding outputs. Five flight modes share the same control law for roll and pitch angles; this fact will be helpful when stability analysis is presented in the next section. The description of each flight mode and its common applications is given below.

Flight modes can be controlled through the radio control (RC) remotely via a transmitter switch, via mission commands, or using commands from a ground control station (GCS) depending on the task we want to fulfill.

3.1. Manual position control mode

Manual position control mode (MP) allows the pilot to fly the quadrotor manually, controlling the roll, pitch, and yaw angles. The RC remote control is used to drive the quadrotor to the desire x and y position through controlling the roll and pitch commands in order to counteract the wind effects. The throttle stick controls the z position of the quadrotor, for heading control, and if the pilot releases the yaw stick, the quadrotor will maintain its current heading.

This flight mode is the standard for almost all the quadrotors in the market because of its intuitive manner to fly the vehicle. Almost all applications need this flight mode in order to have full control on the displacements of the vehicle, but it has its main application in aerial filming. However, the

https://doi.org/10.1017/S0263574720000673 Published online by Cambridge University Press

pilot requires several hours of training to master this flight mode due to the zero dynamics in the x–y plane.

The control objective for manual flight control is to ensure the asymptotic convergence of the variables (x_7, x_9, x_{11}) to the references $(x_{7r}, x_{9r}, x_{11r})$ in (6) by means of U_2, U_3, and U_4.

3.1.1. Roll angle dynamics. Defining the tracking error for roll angles and taken its derivative, we yield to

$$\begin{aligned} z_7 &= x_{7r} - x_7 \\ \dot{z}_7 &= \dot{x}_{7r} - x_8 \\ \ddot{z}_7 &= \ddot{x}_{7r} - \frac{1}{I_x}\left(U_2 + \left(I_y - I_z\right) x_{10}x_{12} + Jx_{10}\omega\right) + A_8. \end{aligned} \tag{7}$$

In order to stabilize the y-dynamics, consider the following exosystem:

$$\ddot{x}_{3r} = \frac{U_1}{m}(-S_{x_{7r}}C_{x_{11}} + C_{x_{7r}}S_{x_{9r}}S_{x_{11}}) - A_4$$

and let define the error

$$\begin{aligned} z_3 &= x_{3r} - x_3 \\ \dot{z}_3 &= \dot{x}_{3r} - x_4 \\ \ddot{z}_3 &= \frac{U_1}{m}(-f_1 C_{x_{11}} + f_2 S_{x_{11}}) \end{aligned}$$

where

$$f_1 = 2\cos\left(\frac{x_{7r} + x_7}{2}\right)\sin\left(\frac{z_7}{2}\right),$$

$$f_2 = \cos\left(\frac{x_{7r} + x_7 + x_{9r} + x_9}{2}\right)\sin\left(\frac{z_7 + z_9}{2}\right) - \cos\left(\frac{x_{7r} + x_7 - x_{9r} - x_9}{2}\right)\sin\left(\frac{z_7 - z_9}{2}\right).$$

Moreover, $\|f_1\| \le \eta\|z_7\| \le 2$, and $\|f_2\| \le \tau_1\|z_7 + z_9\| + \tau_2\|z_7 - z_9\| \le \tau\|z_7\| + \tau\|z_9\| \le 2$. Then, we define the sliding mode surface as

$$\begin{aligned} \sigma_7 &= \dot{z}_7 + k_7 z_7 + C_3 z_3 + C_4 \dot{z}_3 \\ \dot{\sigma}_7 &= \bar{f}_7 - V_7 \end{aligned} \tag{8}$$

with $\bar{f}_7 = \ddot{x}_{7r} - \frac{1}{I_x}\left(\left(I_y - I_z\right) x_{10}x_{12} + Jx_{10}\omega\right) + A_8 + k_7\dot{z}_7 + C_3\dot{z}_3 + C_4\frac{U_1}{m}(-f_1 C_{x_{11}} + f_2 S_{x_{11}})$, $V_7 = \frac{1}{I_x}U_2$, and the constants $k_7, C_3, C_4 > 0$.

3.1.2. Pitch angle dynamics. Define the tracking error for pitch angle

$$\begin{aligned} z_9 &= x_{9r} - x_9 \\ \dot{z}_9 &= \dot{x}_{9r} - x_{10} \\ \ddot{z}_9 &= \ddot{x}_{9r} - \frac{1}{I_y}\left(U_3 + \left(I_z - I_x\right) x_8 x_{12} + Jx_8\omega\right) + A_{10}. \end{aligned} \tag{9}$$

As the same way, define a exosystem

$$\ddot{x}_{1r} = \frac{U_1}{m}(S_{x_{7r}}S_{x_{11}} + C_{x_{7r}}S_{x_{9r}}C_{x_{11}}) - A_2$$

https://doi.org/10.1017/S0263574720000673 Published online by Cambridge University Press

and the error

$$\begin{aligned} z_1 &= x_{1r} - x_1 \\ \dot{z}_1 &= \dot{x}_{1r} - x_2 \\ \ddot{z}_1 &= \frac{U_1}{m}(f_1 S_{x_{11}} + f_2 C_{x_{11}}). \end{aligned}$$

Thus, the sliding mode surface is

$$\begin{aligned} \sigma_9 &= \dot{z}_9 + k_9 z_9 + C_1 z_1 + C_2 \dot{z}_1 \\ \dot{\sigma}_9 &= \bar{f}_9 - V_9 \end{aligned} \tag{10}$$

with $\bar{f}_9 = \ddot{x}_{9r} - \frac{1}{I_y}\left((I_z - I_x)\, x_8 x_{12} + J x_8 \omega\right) + A_{10} + k_9 \dot{z}_9 + C_1 \dot{z}_1 + C_2 \frac{U_1}{m}(f_1 S_{x_{11}} + f_2 C_{x_{11}})$, $V_9 = \frac{1}{I_y} U_3$, and the constants k_9, C_1, $C_2 > 0$.

3.1.3. Yaw angle dynamics. Define the tracking error for yaw angle as

$$\begin{aligned} z_{11} &= x_{11r} - x_{11} \\ \dot{z}_{11} &= \dot{x}_{11r} - x_{12} \\ \ddot{z}_{11} &= \ddot{x}_{11r} - \frac{1}{I_z}\left(U_4 + \left(I_x - I_y\right) x_8 x_{10}\right) + A_{12} \end{aligned} \tag{11}$$

and define the sliding mode surface as

$$\begin{aligned} \sigma_{11} &= \dot{z}_{11} + k_{11} z_{11} \\ \dot{\sigma}_{11} &= \bar{f}_{11} - V_{11} \end{aligned} \tag{12}$$

with $\bar{f}_{11} = \ddot{x}_{11r} - \frac{1}{I_z}\left(U_4 + \left(I_x - I_y\right) x_8 x_{10}\right) + A_{12} + k_{11} \dot{z}_{11}$, $V_{11} = \frac{1}{I_z} U_4$, and $k_{11} > 0$.

In order to make the sliding surfaces converge to zero, we applied the super twisting control algorithm in the Euler angles.

3.1.4. Sliding mode control design for manual position control. From (8), (10), and (12), the projection motion in the subspaces σ_7, σ_9, and σ_{11} is described by

$$\begin{bmatrix} \dot{\sigma}_7 \\ \dot{\sigma}_9 \\ \dot{\sigma}_{11} \end{bmatrix} = \begin{bmatrix} \bar{f}_7 \\ \bar{f}_9 \\ \bar{f}_{11} \end{bmatrix} - \begin{bmatrix} V_7 \\ V_9 \\ V_{11} \end{bmatrix} \tag{13}$$

where

$$\begin{bmatrix} V_7 \\ V_9 \\ V_{11} \end{bmatrix} = B \begin{bmatrix} U_2 \\ U_3 \\ U_4 \end{bmatrix}, \quad B = \begin{bmatrix} \frac{1}{I_x} & 0 & 0 \\ 0 & \frac{1}{I_y} & 0 \\ 0 & 0 & \frac{1}{I_z} \end{bmatrix}. \tag{14}$$

Now, we design the control inputs applying the super twisting control algorithm:[23]

$$\begin{aligned} V_i &= \lambda_i \left|\sigma_i\right|^{1/2} sign(\sigma_i) + \upsilon_i,\ i = 7, 9, 11, \\ \dot{\upsilon}_i &= \alpha_i sign(\sigma_i) \end{aligned} \tag{15}$$

with control gains $\lambda_i > 0$ and $\alpha_i > 0$.

These super twisting controllers ensure the asymptotic tracking of $(x_{7r}, x_{9r}, x_{11r})$. In addition, we define the form of input U_1 as

$$U_1 = \frac{Th_r + m\,(g + Az)}{C_{x7} C_{x9}} \tag{16}$$

https://doi.org/10.1017/S0263574720000673 Published online by Cambridge University Press

where Th_r is a throttle reference based on the limits of the thrust force that can be generated by the four motors and the limits of the RC throttle stick lever.

3.2. Altitude hold mode

In altitude hold mode, the quadrotor maintains a fixed altitude, while roll, pitch, and yaw are available to be manually controlled. In this mode, the variables to control are altitude (z position), roll, pitch, and yaw angles. A barometer, GPS, laser, or a combination of them are needed in order to know the current altitude of the aircraft. In this case, we consider a GPS sensor in which the reference for the absolute position of the quadrotor is generated in a global reference frame. A transformation from this global frame to a local reference frame is carried out in order to handle local trajectories for the absolute position of the quadrotor. This flight mode overcomes the issue of losing thrust force on throttle when displacing along other directions. The most common applications in which this flight mode is useful are all the tasks that require monitoring and inspection of large areas like protected areas, lakes, crops, etc., since the pilot does not have to worry about the altitude of the aircraft while we can move along the x–y plane.

The control objective is to drive the variables (x_5, x_7, x_9, x_{11}) to the reference vector $(x_{5r}, x_{7r}, x_{9r}, x_{11r})$. It can be noted that the controllers for roll, pitch, and yaw angles are the same as in the manual position mode and are described by (15), therefore only the procedure for z position controller must be defined.

3.2.1. z position dynamics. Let us define the tracking error for the altitude position and its dynamics as

$$\begin{aligned} z_5 &= x_{5r} - x_5 \\ \dot{z}_5 &= \dot{x}_{5r} - x_6 \\ \ddot{z}_5 &= \ddot{x}_{5r} - \frac{U_1}{m}\left(C_{x_7} C_{x_9}\right) + g + A_6 \end{aligned} \tag{17}$$

and design the sliding mode surface as

$$\begin{aligned} \sigma_5 &= \dot{z}_5 + k_5 z_5 \\ \dot{\sigma}_5 &= \bar{f}_5 - V_5 \end{aligned} \tag{18}$$

with $\bar{f}_5 = \ddot{x}_{5r} + g + A_6 + k_5 \dot{z}_5$, $V_5 = \frac{C_{x_7} C_{x_9}}{m} U_1$, and $k_5 > 0$.

Since the selection of U_1 will allow us to design smooth sliding manifolds for the x and y displacements, for the other two flight modes we apply the super twisting control algorithm with a sigmoid function as follows:

$$\begin{aligned} V_5 &= \lambda_5 \left|\sigma_5\right|^{1/2} sigm(\varepsilon_5, \sigma_5) + \upsilon_5 \\ \dot{\upsilon}_5 &= \alpha_5 sign(\sigma_5) \end{aligned} \tag{19}$$

with control gains $\lambda_5 > 0$ and $\alpha_5 > 0$. The sigmoid function used in this work is defined as in ref. [24]

$$sigm(\varepsilon, \sigma) = tanh(\varepsilon\sigma). \tag{20}$$

3.3. GPS-fixed mode (L)

The GPS-fixed mode automatically maintains the current location (longitude, latitude, and altitude) and the heading of the quadrotor. The pilot may change the orientation about the z axis (yaw angle) via the RC remote control.

This flight mode is useful for applications like search and rescue, forest fire detection, and monitoring and inspection of infrastructure tasks because the pilot can command, through the RC remote control, the quadrotor to hold its current position when it detects an object of interest.

https://doi.org/10.1017/S0263574720000673 Published online by Cambridge University Press

The control objective is to drive the variables (x_1, x_3, x_5, x_{11}) to the reference vector $(x_{1r}, x_{3r}, x_{5r}, x_{11r})$. It can be noted that the controllers for roll, pitch, yaw angles, and z position are the same as in the MP and altitude control mode and are described by (15) and (18). Therefore, only the longitude (x position) and latitude (y position) controllers have to be designed.

3.3.1. x position dynamics. To follow a desired longitudinal position, we define the tracking error and its dynamics as

$$\begin{aligned} z_1 &= x_{1r} - x_1 \\ \dot{z}_1 &= \dot{x}_{1r} - x_2 \\ \ddot{z}_1 &= \ddot{x}_{1r} - \frac{U_1}{m}\left(S_{x_7}S_{x_{11}} + C_{x_7}S_{x_9}C_{x_{11}}\right) + A_2 \end{aligned} \tag{21}$$

Applying the block control technique, we define the pseudo control $U_x = S_{x_7}S_{x_{11}} + C_{x_7}S_{x_9}C_{x_{11}}$, because the input U_1 has been already assigned to the dynamics of z position, this means that there exists a relation between the roll, pitch, and yaw angles. Moreover, the translations in x and y directions depended on these angles. Then, we can define the sliding mode surface as

$$\begin{aligned} \sigma_1 &= \dot{z}_1 + k_1 z_1 \\ \dot{\sigma}_1 &= \bar{f}_1 - V_1 \end{aligned} \tag{22}$$

with $\bar{f}_1 = \ddot{x}_{1r} + A_2 + k_1\dot{z}_1$, $V_1 = -\frac{U_1}{m}U_x$, and $k_1 > 0$.

3.3.2. y position dynamics. To follow a desired latitudinal position, we define the tracking error and its dynamics as

$$\begin{aligned} z_3 &= x_{3r} - x_3 \\ \dot{z}_3 &= \dot{x}_{3r} - x_4 \\ \ddot{z}_3 &= \ddot{x}_{3r} - \frac{U_1}{m}\left(-S_{x_7}C_{x_{11}} + C_{x_7}S_{x_9}S_{x_{11}}\right) + A_4 \end{aligned} \tag{23}$$

Let us define the pseudo control $U_y = -S_{x_7}C_{x_{11}} + C_{x_7}S_{x_9}S_{x_{11}}$ and propose the next sliding mode surface

$$\begin{aligned} \sigma_3 &= \dot{z}_3 + k_3 z_3 \\ \dot{\sigma}_3 &= \bar{f}_3 - V_3 \end{aligned} \tag{24}$$

with $\bar{f}_3 = \ddot{x}_{3r} + A_y + k_3\dot{z}_3$, $V_3 = -\frac{U_1}{m}U_y$, and $k_3 > 0$.

3.3.3. Sliding mode control design for GPS-fixed mode. Now, we can apply the super twisting control algorithm with the sigmoid function as in (19)

$$\begin{aligned} V_i &= \lambda_i |\sigma_i|^{1/2} sigm(\varepsilon_i, \sigma_i) + \upsilon_i, \quad i = 1, 3, \\ \dot{\upsilon}_i &= \alpha_i sign(\sigma_i) \end{aligned} \tag{25}$$

with control gains $\lambda_i > 0$ and $\alpha_i > 0$.

So far, we have generated a smooth form of the pseudo controls U_x and U_y. On the other hand, the references in x and y position will give us the desired U_x and U_y, then

$$\begin{aligned} U_{xd} &= S_{x_{7d}}S_{x_{11}} + C_{x_{7d}}S_{x_{9d}}C_{x_{11}} \\ U_{yd} &= -S_{x_{7d}}C_{x_{11}} + C_{x_{7d}}S_{x_{9d}}S_{x_{11}} \end{aligned} \tag{26}$$

Therefore, the problem of following desired x and y position is reduced to follow desired roll and pitch angles, which can be achieved by the laws of control defined in (15). But first, we have to decouple x_{7d} and x_{9d} from the linear combination which is nonsingular for all x_{11}, and the solution

https://doi.org/10.1017/S0263574720000673 Published online by Cambridge University Press

for x_{7d} and x_{9d} is contained in $(-\pi/2, \pi/2)$, therefore

$$\begin{aligned} x_{7d} &= \arcsin(U_{xd}S_{x_{11}} + U_{yd}C_{x_{11}}) \\ x_{9d} &= \arcsin\left(\frac{U_{xd}C_{x_{11}} - U_{yd}S_{x_{11}}}{C(x_{7d})}\right) \end{aligned} \tag{27}$$

Now, we assign $x_{7r} = x_{7d}$ and $x_{9r} = x_{9d}$ and use the equations in (15) to achieve the convergence of these angles.

3.4. Autonomous control mode (A)

In autonomous control mode, the quadrotor will use predefined way points to follow a desired trajectory. This is done via a ground station, while the RC remote control is used to activate the mission. The applications that can be fulfilled with this flight mode are drone-based delivery system, ambulance drone, surveillance, among others.

The objective control variables are the same than that in the GPS-fixed mode $(x_{1r}, x_{3r}, x_{5r}, x_{11r})$, but the main difference is that the references are generated from a user via a ground station or autonomously from path planning algorithm. The only assumption is that the generated trajectories must be smooth functions of time at least of class C^2.

3.5. Manual velocity control mode

In this flight mode, the user can manually control the velocity of the aircraft (x_2, x_4, x_6, x_{12}) through RC commands. This mode is designed for those users without enough flight experience, allowing new users to fly in an easier and safer way. The throttle stick controls the velocity of the quadrotor in the z-axis, the yaw stick now commands the yaw velocity and not the position, as it is in the manual position mode. The roll and pitch references now become velocity references for displacements in the x- and y- axis, respectively.

The control objective is to drive the variables (x_2, x_4, x_6, x_{12}) to the reference vector $(x_{2r}, x_{4r}, x_{6r}, x_{12r})$. It can be noted that the procedure is similar to the position control in the GPS-fixed and autonomous control modes, with the difference that now the outputs of the system have reduced the relative degree of the system, which makes the design of surfaces much simpler for the sliding mode controllers.

3.5.1. z velocity dynamics. Let us define the tracking error for the altitude velocity and its dynamics as

$$\begin{aligned} z_6 &= x_{6r} - x_6 \\ \dot{z}_6 &= \dot{x}_{6r} - \frac{U_1}{m}\left(C_{x_7}C_{x_9}\right) + g + A_6 \end{aligned} \tag{28}$$

and design the sliding mode surface as

$$\begin{aligned} \sigma_6 &= z_6 \\ \dot{\sigma}_6 &= \bar{f}_6 - V_6 \end{aligned} \tag{29}$$

with $\bar{f}_6 = \dot{x}_{6r} + g + A_6$ and $V_6 = \frac{C_{x_7}C_{x_9}}{m}U_1$.

Using the super twisting control algorithm with the sigmoid function as in (19)

$$\begin{aligned} V_6 &= \lambda_6 |\sigma_6|^{1/2} sigm(\varepsilon_6, \sigma_6) + \upsilon_6 \\ \dot{\upsilon}_6 &= \alpha_6 sign(\sigma_6) \end{aligned} \tag{30}$$

with control gains $\lambda_6 > 0$ and $\alpha_6 > 0$.

https://doi.org/10.1017/S0263574720000673 Published online by Cambridge University Press

3.5.2. x velocity dynamics. To follow a desired longitudinal velocity, we define the tracking error and its dynamics as

$$\begin{aligned} z_2 &= x_{2r} - x_2 \\ \dot{z}_2 &= \dot{x}_{2r} - \frac{U_1}{m}\left(S_{x_7}S_{x_{11}} + C_{x_7}S_{x_9}C_{x_{11}}\right) + A_2 \end{aligned} \tag{31}$$

As in the GPS-fixed mode, we define the pseudo control $U_x = S_{x_7}S_{x_{11}} + C_{x_7}S_{x_9}C_{x_{11}}$. Then, we define the sliding mode surface as

$$\begin{aligned} \sigma_2 &= \dot{z}_2 \\ \dot{\sigma}_2 &= \bar{f}_2 - V_2 \end{aligned} \tag{32}$$

with $\bar{f}_2 = \dot{x}_{2r} + A_2$ and $V_2 = -\frac{U_1}{m}U_x$.

3.5.3. y velocity dynamics. To follow a desired latitudinal velocity, we define the tracking error and its dynamics as

$$\begin{aligned} z_4 &= x_{4r} - x_4 \\ \dot{z}_4 &= \dot{x}_{4r} - \frac{U_1}{m}\left(-S_{x_7}C_{x_{11}} + C_{x_7}S_{x_9}S_{x_{11}}\right) + A_4 \end{aligned} \tag{33}$$

Let us define the pseudo control $U_y = -S_{x_7}C_{x_{11}} + C_{x_7}S_{x_9}S_{x_{11}}$ and propose the next sliding mode surface

$$\begin{aligned} \sigma_4 &= \dot{z}_4 \\ \dot{\sigma}_4 &= \bar{f}_4 - V_4 \end{aligned} \tag{34}$$

with $\bar{f}_4 = \dot{x}_{4r} + A_y$ and $V_3 = -\frac{U_1}{m}U_y$.

3.5.4. Sliding mode control design for manual velocity mode. Now, we can apply the super twisting control algorithm with the sigmoid function as in (19)

$$\begin{aligned} V_i &= \lambda_i \left|\sigma_i\right|^{1/2} sigm(\varepsilon_i, \sigma_i) + \upsilon_i, \quad i = 2, 4, \\ \dot{\upsilon}_i &= \alpha_i sign(\sigma_i) \end{aligned} \tag{35}$$

with control gains $\lambda_i > 0$ and $\alpha_i > 0$. This let us generate the pseudo controls U_x and U_y. Now we use (26) and (27) to assign $x_{7r} = x_{7d}$ and $x_{9r} = x_{9d}$ and use the equations in (15) for achieving the convergence of these angles.

3.6. Return to home (H)

The flight mode return to home navigates the quadrotor from its current absolute position to hover above the home position. The reference is generated in this flight mode, and it is sent to the autonomous mode with $(x_{1r}, x_{3r}, x_{5r}, x_{11r})$. These references are defined as

$$\begin{aligned} x_{1r} &= x_{home} \\ x_{3r} &= y_{home} \\ x_{5r} &= \begin{cases} z_H & if\ x \neq x_{home}, y \neq y_{home} \\ z_{home} & else \end{cases} \\ x_{11r} &= yaw_H \end{aligned} \tag{36}$$

where z_H and yaw_H are the values of z and yaw when the mode H is activated.

https://doi.org/10.1017/S0263574720000673 Published online by Cambridge University Press

4. Closed-Loop Stability

In this section, the stability analysis of the proposed multimode flight framework is developed. First, we will state the stability proof for the complete system, without taking into account the transition from one flight mode to another. This will be carried out later.

4.1. Sliding mode stability

In order to establish the sliding mode stability condition for the Euler angles, we rewrite (13) with (15) as

$$\begin{aligned} \dot{\sigma}_i &= \bar{f}_i - \lambda_i \left|\sigma_i\right|^{1/2} sign(\sigma_i) + \sigma_{i+1}, \quad i = 1, 2, 3, 4, 5, 6, 7, 9, 11, \\ \dot{\sigma}_{i+1} &= \alpha_i sign(\sigma_i). \end{aligned} \tag{37}$$

Now, we introduce the following assumption:

Assumption 4.1. *The perturbation term $\bar{f}_i$ is bounded in an admissible operation region D_1 by*

$$\left|f_i\right| \leq \delta_i \left|\sigma_i\right|^{1/2}, \quad i = 1, 2, 3, 4, 5, 6, 7, 9, 11, \tag{38}$$

with constants $\delta_i > 0$.

Then, we can state the following theorem which assures the robustness of the convergence of the trajectory error to zero in finite time.

Theorem 1. [25] *Under Assumption 4.1, the origin $\sigma_i = 0$ is a locally asymptotically stable equilibrium point if the controller gains λ_i and α_i satisfy*

$$\begin{aligned} \lambda_i &> 2\bar{f}_i \\ \alpha_i &> \lambda_i \frac{5\bar{f}_i\lambda_i + 4\bar{f}_i^2}{2\left(\lambda_i - 2\bar{f}_i\right)}. \end{aligned} \tag{39}$$

Moreover, all trajectories converge to the origin in finite time, upperbounded by $T = \frac{2V_i^{1/2}(\sigma_{i_0})}{\gamma_i}$, where s_{i_0} is the initial state and γ_i is a constant depending on the controller gains and the perturbation term.

Then, we use (19) and rewrite (25) with (22)–(22) in order to establish the sliding mode stability condition for the x, y, and z positions, but first we introduce the following assumptions:

Assumption 4.2. *The sign function can be approximated by the sigmoid function as shown by the following limit:*

$$\lim_{\varepsilon \to \infty} sigm(\varepsilon_i, \sigma_i) = sign(\sigma_i) \tag{40}$$

Assumption 4.3. *Let us define the difference between sign and sigmoid function for a given ε by*

$$\Delta(\varepsilon_i, \sigma_i) = sign(\sigma_i) - sigm(\varepsilon_i, \sigma_i) \tag{41}$$

and $\Delta(\varepsilon_i, \sigma_i)$ is bounded, that is, there exists a positive constant ϱ such that

$$\left\|\Delta(\varepsilon_i, \sigma_i)\right\| \leq \varrho_i \leq 1 \tag{42}$$

Theorem 2. *Under Assumption 1, the origin $s_i = 0$ is a locally asymptotically stable equilibrium point if the controller gains λ_i and α_i satisfy*[24]

$$\begin{aligned} \lambda_i &> \tfrac{2\bar{f}_i}{1-\varrho_i} \\ \alpha_i &> \lambda_i \tfrac{5\bar{f}_i\lambda_i + 4\bar{f}_i^2}{2(\lambda_i - 2\bar{f}_i).} \end{aligned} \tag{43}$$

https://doi.org/10.1017/S0263574720000673 Published online by Cambridge University Press

4.2. Stability for switching flight modes

The problem considered in this work assumes that the occurrence of transitions between flight modes is determined by a switching signal $\rho(t)$. Each flight mode defines the current nonlinear closed-loop system of the quadrotor. This switching signal cannot be specified a priori because it is defined by the user of the quadrotor or depending on characteristics of the environment. So, in order to demonstrate the stability of the global nonlinear switching closed-loop system, we use the common Lyapunov function principle.[26] Let us define the stability conditions with the following theorem:

Theorem 3. *Under Assumptions 4.1, 4.2, and 4.3, the origin of the error dynamics of the closed-loop system defined by (6), $U_1 - U_4$, and $\rho(t)$ is a locally asymptotically stable equilibrium point if the controller gains α_i and λi satisfy the conditions (43), regardless of the switching function $\rho(t)$.*

Proof. It is easy to see that conditions (43) assure the fulfillment of conditions (39). Then, there exists a common positive-definite Lyapunov function for each block defined as:[24]

$$V(\sigma) = \Psi^T P \Psi \tag{44}$$

where

$$\Psi^T = \begin{bmatrix} |\sigma_i|^{\frac{1}{2}} \, sign(\sigma_i) & \sigma_i \end{bmatrix}, P = \frac{1}{2}\begin{bmatrix} 4\alpha + \lambda^2 & -\lambda \\ -\lambda & 2 \end{bmatrix} \tag{45}$$

and $\lambda > \lambda_i$, $\alpha > \alpha_i$ associated with $F = \sup\{\bar{f}_i\}$ for all i of the flight modes considered in this work. Its derivative is obtained as

$$\dot{V}(\sigma_i) = -\frac{1}{|\sigma_i|^{\frac{1}{2}}} \Psi^T Q \Psi + \frac{F}{|\sigma_i|^{\frac{1}{2}}} q^T \Psi \tag{46}$$

with

$$Q = \frac{\lambda}{2}\begin{bmatrix} 2\alpha + \lambda^2 & -\lambda \\ -\lambda & -1 \end{bmatrix} \tag{47}$$

and

$$q^T = \begin{bmatrix} 2\alpha + \frac{\lambda^2}{2} & -\frac{\lambda}{2} \end{bmatrix} \tag{48}$$

which is a negative semidefinite function under conditions (43). Hence, the origin of the error dynamics of the global nonlinear switching closed-loop system is locally asymptotically stable.[26] For further details on the demonstration, please refer to ref. [10].

5. Simulation Results

In order to verify the effectiveness of the proposed control scheme, the following case of study is considered. The experiment simulates a forest fire detection task. This task could involve several flight modes for a better user experience.

The forest is monitored and inspected with a quadrotor which is configured with the flight modes: autonomous, manual velocity, GPS fixed, and return to home, associated with the states A, MV, L, and H, respectively. Additionally, the Idle state I, that is the initial mode, is added as depicted in Fig. 1.

Flight modes are controlled through a transmitter switch in the RC remote control and via a mission command when the infrared camera detects a hot spot; these events are a, h, j, and m activating the states A, H, L, and MV, respectively. Uncontrollable events are l and s, due to casual to detect a hot spot in the forest and to stop the aircraft, which in turn activate the states of interest L and I, respectively. It can be noted that the machine is controllable if the combination of possible controllable words, concatenates with uncontrollable events, which in turn are in the state machine, can be generated with controllable words, that is, if the controllable words are

$$K = \{\overline{almhs}, \overline{malmhs}, \overline{mjalhs}\}, \tag{49}$$

https://doi.org/10.1017/S0263574720000673 Published online by Cambridge University Press

Table I. Simulation parameters

Parameter	Value	Unit
m	1.26	Kg
d	0.23	m
I_x	5.5×10^{-3}	kg m^2
I_y	5.5×10^{-3}	kg m^2
I_z	11×10^{-3}	kg m^2
J	1.46×10^{-3}	kg m^2
b	9.4168×10^{-6}	N s^2/rad^2
c	2.4483×10^{-7}	Nm s^2/rad^2
g	9.81	m/s^2

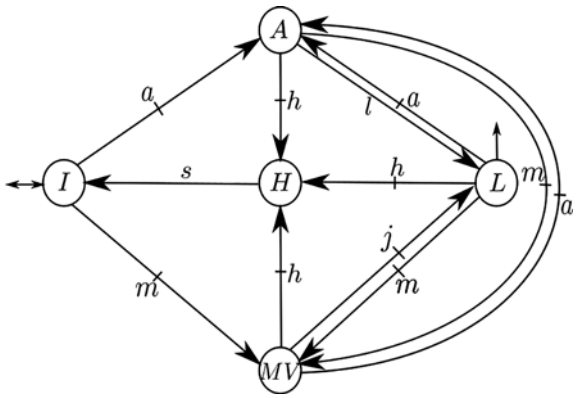


Fig. 1. State machine for switching control.

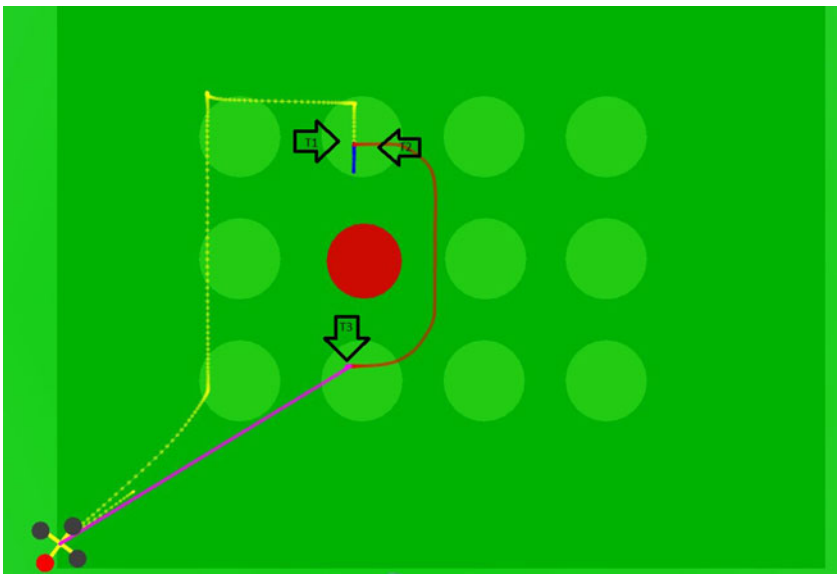


Fig. 2. Aerial view of the flight performance. The transition between the stages T1, T2, and T3 is described by the controllable word $\overline{almhs}$.

where $\overline{(\cdot)}$ is the repetition of the argument many times as necessary, and uncontrollable words are $\Sigma_u = \{s, l\}$[27]

$$\bar{K}\Sigma_u \cap L_m \in \bar{K}$$

https://doi.org/10.1017/S0263574720000673 Published online by Cambridge University Press

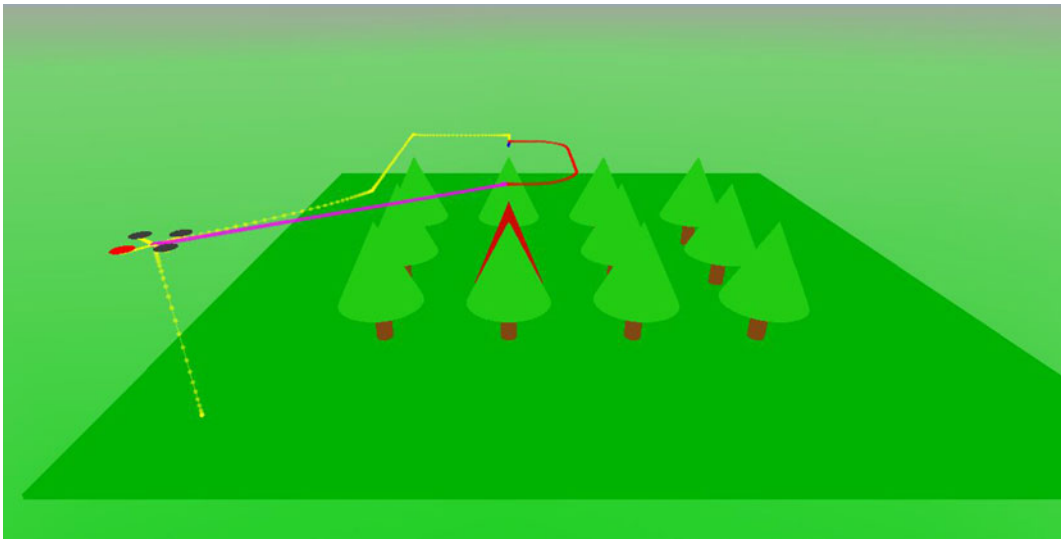


Fig. 3. Lateral view of the flight performance.

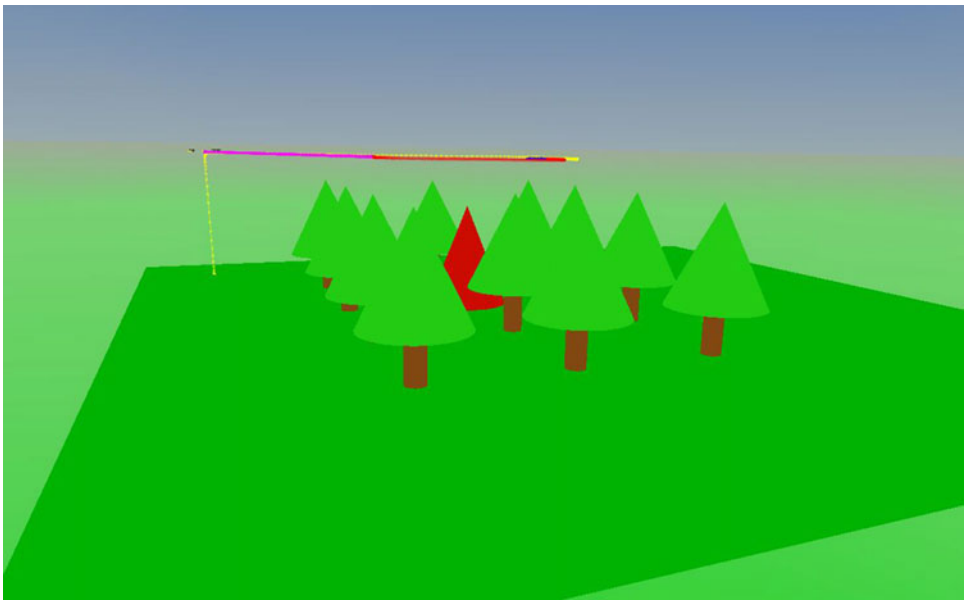


Fig. 4. Lateral view of the flight performance.

where L_m is the language that launches the interest states $L_m = \{\overline{al}\,\overline{malhs}, \overline{mal}\,\overline{al}, \overline{malmhs}, \overline{almhs}, \overline{al}\,\overline{mj}, \overline{mj}\,\overline{alhs}\}$. Finally, it is easy to confirm that such control is not blocking, that is, if the words can be generated with the control, which are in the words of the state machine of interest, they are in control. In other words,

$$\bar{K} \cap L_m = \{\overline{almhs}, \overline{malmhs}, \overline{mjalhs}\} = K$$

then K is not blocking for the system considered for the inspection.

A 3D environment has been developed in simulink, and also the plant was modeled according to (6) with the parameters measured from a quadrotor prototype built in Cinvestav Guadalajara, which are listed in Table I. The solver used in the simulation is ode1(Euler) with a fixed step size of 0.001 s. The gains of the controller are $\lambda_i = [10, 10, 5, 15, 15, 5]$ and $\alpha_i = [10, 10, 1, 5, 5, 1]$, $i = 1, 3, 5, 7, 9, 11$.

Each flight mode can be identified by a color in the picture: yellow for autonomous control mode (A), blue for GPS fixed mode (L), red for MV, and purple for the return to home mode (H). The

https://doi.org/10.1017/S0263574720000673 Published online by Cambridge University Press

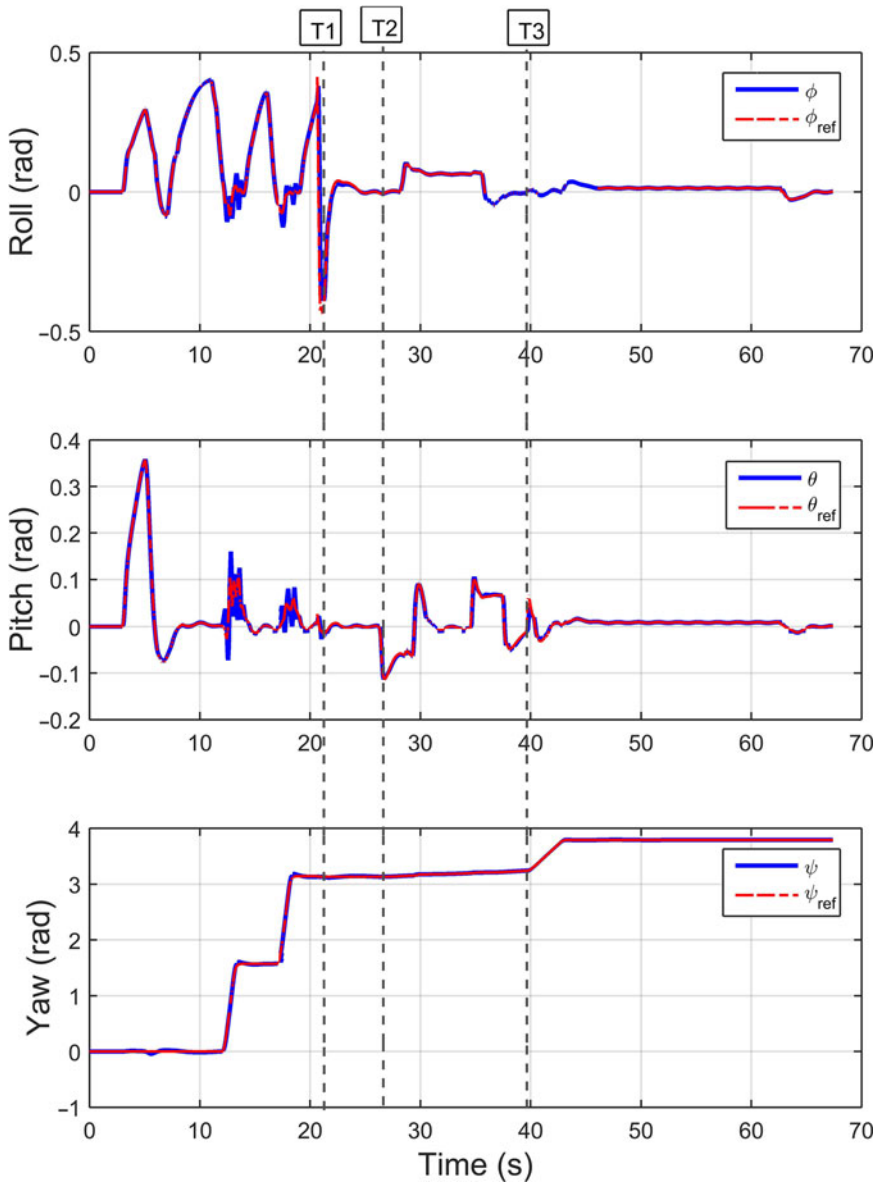


Fig. 5. Euler angles of the quadrotor's pose during the experiment. The convergence of the angles to their respective reference can be noted for all the flight modes.

simulation involves four stages: (1) the UAV performs an autonomous flight mode for taking-off and following a predefined inspection trajectory, (2) a fire is detected after 21 s of simulation and the UAV switches to GPS-F mode, (3) in this stage, the UAV sends/saves information about the fire (position, temperature range, and dimensions) and the user switches to MV, moving the quadrotor manually around the fire area, (4) once the UAV is out of risk, the user decides to return the UAV to the base using the return to home mode. The switching between these stages occur: T1 from (1) to (2) at 21 s, T2 from (2) to (3) at 26 s, and T3 from (3) to (4) at 40 s. It is worth to note that the transitions between the stages during the simulation are described by the controllable word $\overline{almhs}$, which is generated by means of the state machine for the different flight modes described in Fig. 1. Also, in all the flight time, the perturbations were null, except on the interval $t_{pert} = [35, 55]$ s when an external wind perturbation with a speed of 3 m/s in east–west direction is applied.

As we can see from Figs. 2, 3, and 4, a good trajectory tracking has been performed in the autonomous mode. Also, the transitions between flight modes are achieved holding the same altitude and performing a stable flight.

https://doi.org/10.1017/S0263574720000673 Published online by Cambridge University Press

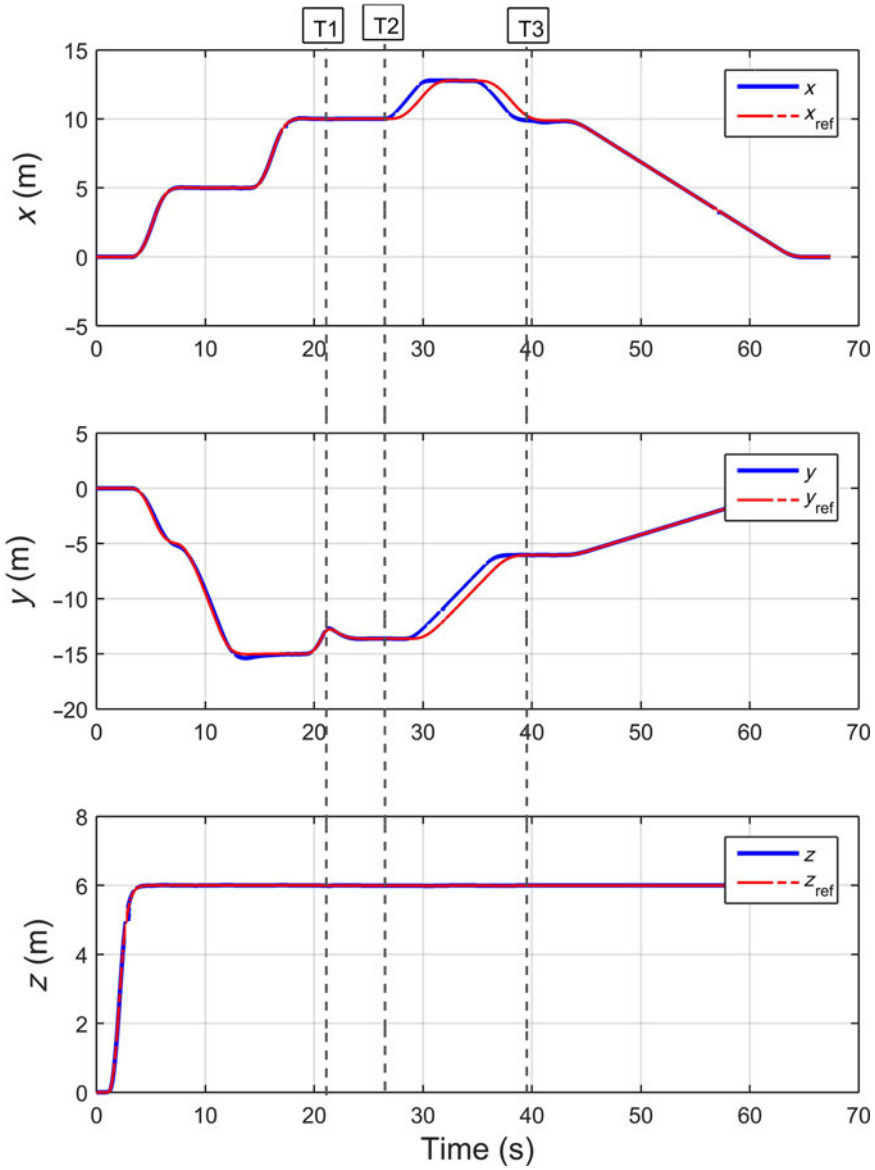


Fig. 6. 3D coordinates of the quadrotor during the experiment. The correct tracking of the reference signals can be appreciated.

It can be noted that in Fig. 5 the controller for the attitude angles described in (15) is always running.

Also, we can see in Fig. 5 a good tracking of the desired attitude angles of the aircraft that yields to a good tracking of the desired position for the quadrotor, as demonstrated in Fig. 6. Besides, as we explained in the flight modes section, the case of study for the $x - y$ position only occurs during the GPS-fixed or autonomous modes, so in order to analyze the position tracking properly, we need to take into account when $t = [0, 26]$ and when $t = [40, 70]$ from Fig. 6.

From Figs. 7 and 8, we can confirm that the forces are within the capabilities of the motors. A second-order transfer function was implemented simulating the dynamics of each one of the motors in order to see if they were capable to follow the control laws. Based on the simulation results, the control compensates this unmodeled dynamic without loosing robustness, which is one of the advantages of this approach.

https://doi.org/10.1017/S0263574720000673 Published online by Cambridge University Press

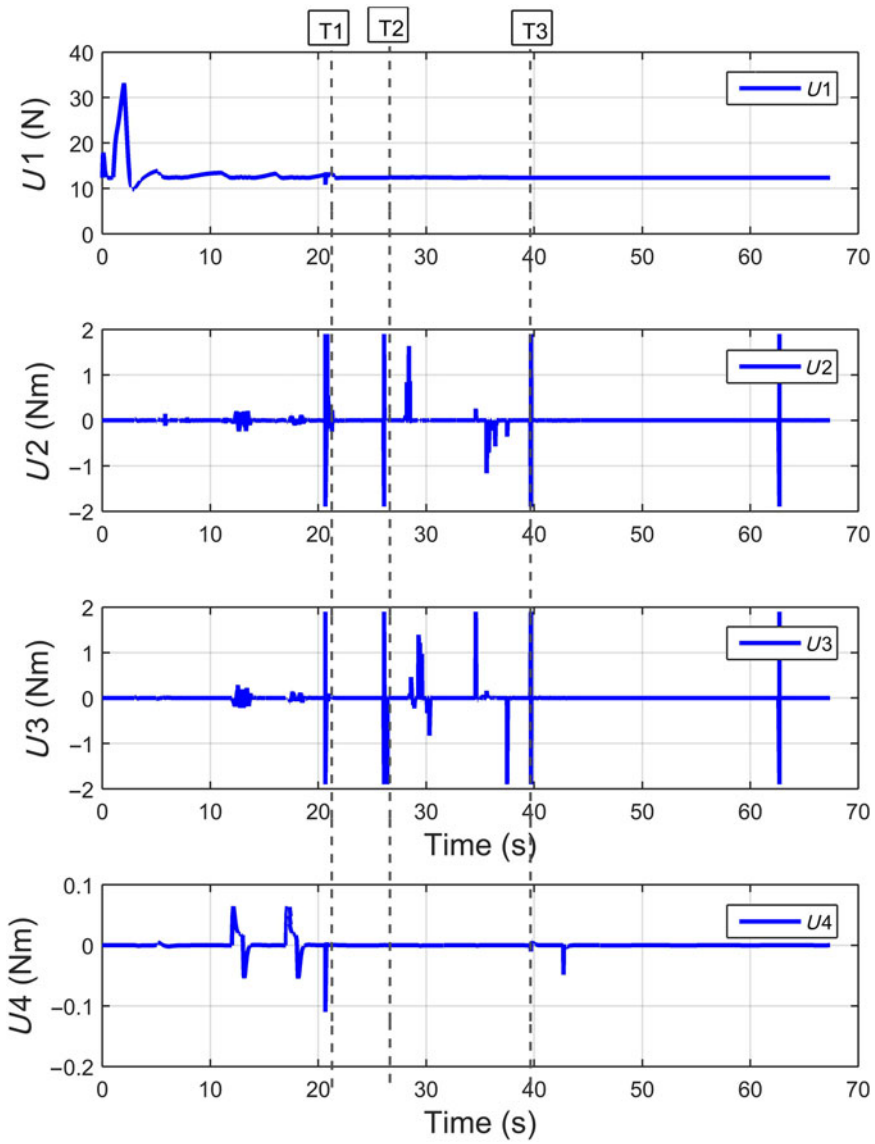


Fig. 7. Control terms generated during the simulation.

6. Conclusions

In this paper, we have proposed a framework for a multimode flight robust control system for a quadrotor based on the super twisting algorithm and the block control technique. The flight modes considered in the control scheme are manual position, altitude hold, GPS fixed, autonomous manual velocity mode, and return to home. The control design for each flight mode is developed, and the stability analysis for the closed-loop system in each case was carried out. In addition, the stability for the global switched nonlinear system was demonstrated by means of the concept of a common Lyapunov function for all the flight modes.

The simulation experiments showed the performance of the proposed control scheme, and it encompassed various transitions between flight modes. It can be noted that the super twisting algorithm permitted to obtain robust chattering-free control signals with a low stabilization period. This control scheme asymptotically tracks the references needed for each flight mode. Moreover, it gives the possibility to perform more complete tasks when different flight modes are required. These features are highly desired in almost every UAV application. Currently, real-time implementation of the proposed control scheme is carried out at LAVAT in Cinvestav.

https://doi.org/10.1017/S0263574720000673 Published online by Cambridge University Press

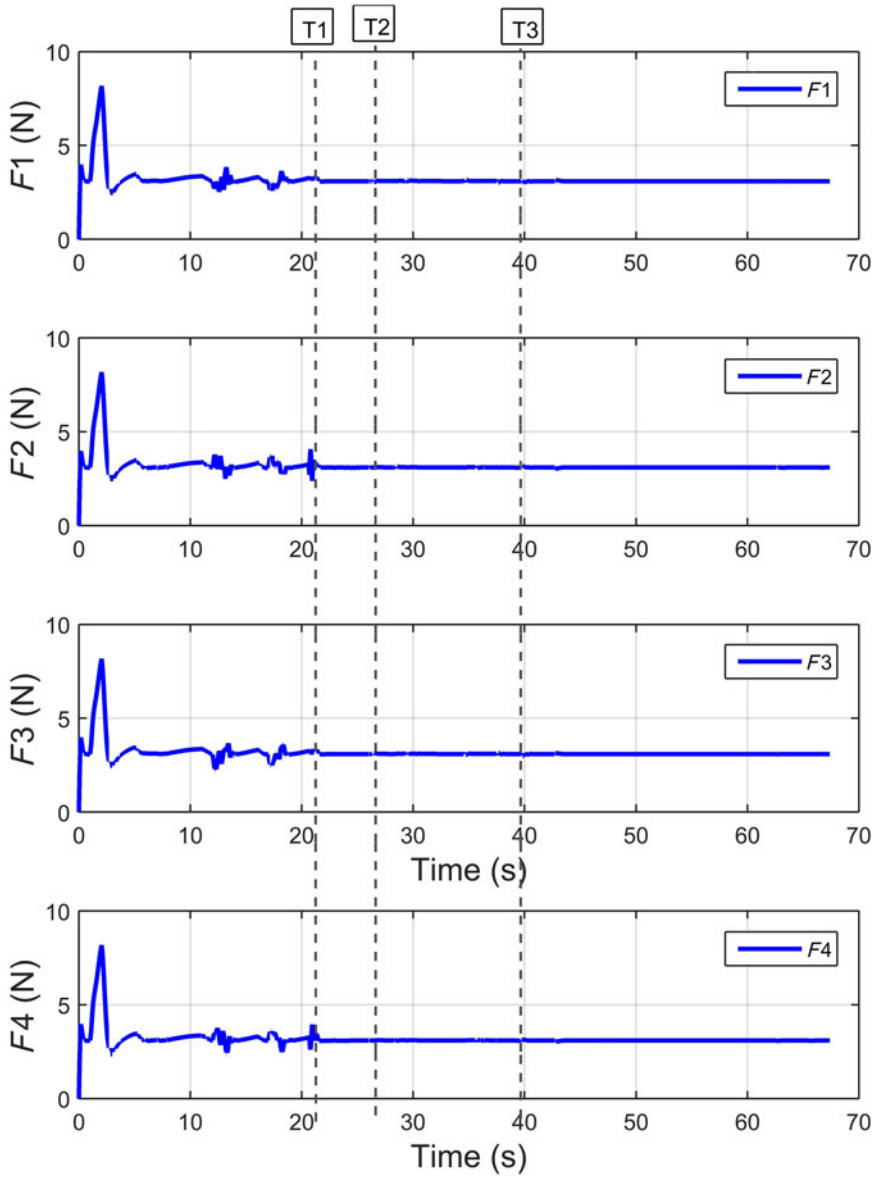


Fig. 8. Thrust forces generated by the propellers during the experiment.

Acknowledgments

The authors would like to thank the National Council on Science and Technology (CONACyT) for supporting this research under grant 300573.

References

1. P. Castillo, A. Dzul and R. Lozano, "Real-time stabilization and tracking of a four-rotor mini rotorcraft," *IEEE Trans. Cont. Sys. Tech.* **4**(12), 510–516 (2004).
2. L. Derafa, L. Fridman, A. Benallegue and A. Ouldali, "Super Twisting Control Algorithm for the Four Rotors Helicopter Attitude Tracking Problem," *Proceedings of the 11th International Workshop on Variable Structure Systems (VSS)* (2010) pp. 62–67.
3. A. Rabhi, M. Chadli and C. Pegard, "Robust Fuzzy Control for Stabilization of a Quadrotor," *Proceedings of the 15th International Conference on Advanced Robotics (ICAR)* (2011) pp. 471–475.
4. H. Khebbache, B. Sait, F. Yacef and Y. Soukkou, "Robust stabilization of a quadrotor aerial vehicle in presence of actuator faults," *IJITCA* **2**(2), 1–13 (2012).
5. T. Madani and A. Benallegue, "Backstepping Control with Exact 2-Sliding Mode Estimation for a Quadrotor Unmanned Aerial Vehicle," *Proceedings of the IEEE/RSJ International Conference on Intelligent Robots and Systems 2007* (2007) pp. 141–146.

https://doi.org/10.1017/S0263574720000673 Published online by Cambridge University Press

6. A. Benallegue, A. Mokhtari and L. Fridman, "Feedback Linearization and High Order Sliding Mode Observer for a Quadrotor UAV," *Proceedings of the International Workshop on Variable Structure Systems* (2006) pp. 365–372.
7. T. Madani and A. Benallegue, "Sliding Mode Observer and Backstepping Control for a Quadrotor Unmanned Aerial Vehicles," *Proceedings of the American Control Conference '07* (2007) pp. 5887–5892.
8. S. Stevanovic, J. Kasac and J. Stepanic, "Robust Tracking Control of a Quadrotor Helicopter without Velocity Measurement," *23rd International DAAAM Symposium* (2012) pp. 595–600.
9. S. Islam, P. Liu and A. Saddik, "Nonlinear robust adaptive sliding mode control design for miniature unmanned multirotor aerial vehicle," *Int. J. Control Autom. Syst.* **15**(10), 1–8 (2017).
10. J. Zhang, Q. Li, N. Cheng and B. Liang, "Non-linear flight control for unmanned aerial vehicles using adaptive backstepping based on invariant manifolds," *J. Aerospace Eng.* **1**(227), 33–44 (2013).
11. M. Basri, "Trajectory tracking control of autonomous quadrotor helicopter using robust neural adaptive backstepping approach," *J. Aerospace Eng.* **21**(2), 1–15 (2018).
12. H. Razmi and S. Afshinfar, "Neural network-based adaptive sliding mode control design for position and attitude control of a quadrotor UAV," *Aerospace Sci. Tech.* **91**, 12–27 (2019).
13. C. Zhang, X. Zhou, H. Zhao, A. Dai and H. Zhou, "Three-Dimensional Fuzzy Control of Mini Quadrotor UAV Trajectory Tracking Under Impact of Wind Disturbance", *Proceedings of the 2016 International Conference on Advanced Mechatronic Systems* (2016) pp. 372–377.
14. Y. Zou and Z. Meng, "Immersion and invariance-based adaptive controller for quadrotor systems," *IEEE Trans. Syst. Man Cybern. Syst.* **49**(11), 2288–2297 (2018).
15. T. Jiang, T. Song and D. Lin, "Integral sliding mode based control for quadrotors with disturbances: Simulations and experiments," *Int. J. Control Autom. Syst.* **17**(8), 1987–1998 (2019).
16. D. Redrovan and D. Kim, "Multiple Quadrotors Flight Formation Control Based on Sliding Mode Control and Trajectory Tracking," *Proceedings of the 2018 International Conference on Electronics, Information, and Communication (ICEIC)* (2018) pp. 1–6.
17. http://copter.ardupilot.com/wiki/flight-modes.
18. L. Bo and L. Ping, "A Stateflow Based Simulation of UAV Multi-mode Flight Control," *Proceedings of the 8th World Congress on Intelligent Control and Automation* (2010) pp. 3347–3352.
19. X. Hongzhe, H. Jim and Z. Yaoming, "Design of Multi-mode Flight Control System for Unmanned Helicopter," *Proceedings of the 30th Chinese Control Conference* (2011) pp. 3660–3663.
20. J. Boskovic and R. Mehra, "Multi-mode Switching in Flight Control," *Proceedings of the The 19th Digital Avionics Systems Conference* (2000) pp. 6F2/1–6F2/8.
21. A. Villanueva, B. Castillo-Toledo, E. Bayro-Corrochano, L. F. Luque-Vega and L. E. Gonzalez-Jimenez, "Multi-mode Flight Sliding Mode Control System for a Quadrotor," *Proceedings of the 2015 International Conference on Unmanned Aircraft Systems (ICUAS)*, Denver, CO (2015) pp. 861–870.
22. S. Bouabdallah, P. Murrieri and R. Siegwart, "Design and Control of an Indoor Micro Quadrotor," *Proceedings of the IEEE International Conference on Robotics and Automation (ICRA'04)* (2004) pp. 4393–4398.
23. A. Levant, "Universal single-input-single-output (SISO) sliding-mode controllers with finite-time convergence," *IEEE Trans. Aut. Cont.* **9**(46), 1447–1451 (2001).
24. L. Gonzalez-Jimenez, A. Loukianov and E. Bayro-Corrochano, "Fully Nested Super-Twisting Algorithm for Uncertain Robotic Manipulators," *Proceedings of the 2011 IEEE International Conference on Robotics and Automation* (2011) pp. 5807–5812.
25. J. Moreno and M. Osorio, "A Lyapunov Approach to Second-Order Sliding Mode Controllers and Observers," *Proceedings of the 47th IEEE Conference on Decision and Control* (2008) pp. 2856–2861.
26. E. Moulay, R. Bourdaisa and W. Perruquetti, "Stabilization of nonlinear switched systems using control Lyapunov functions," *Nonlinear Anal. Hybrid Syst.* **4**(1), 482–490 (2007).
27. W. Murray Wonham and Kai Cai, *Supervisory Control of Discrete-Event Systems*, 1st edn. (Springer International Publishing, Switzerland, 2019).

https://doi.org/10.1017/S0263574720000673 Published online by Cambridge University Press